Optical design considerations and raytracing results for the Arcus grating spectrometer concept

Ryan Allured, Randall L. McEntaffer, Edward Hertz, Peter N. Cheimets, Randall K. Smith

Ryan Allured, Randall L. McEntaffer, Edward Hertz, Peter N. Cheimets, Randall K. Smith, "Optical design considerations and raytracing results for the Arcus grating spectrometer concept," Proc. SPIE 9905, Space Telescopes and Instrumentation 2016: Ultraviolet to Gamma Ray, 99054O (17 August 2016); doi: 10.1117/12.2233763

Event: SPIE Astronomical Telescopes + Instrumentation, 2016, Edinburgh, United Kingdom

Optical design considerations and raytracing results for the Arcus grating spectrometer concept

Ryan Allured[a], Randall L. McEntaffer[b], Edward Hertz[a], Peter N. Cheimets[a], and Randall K. Smith[a]

[a]Harvard-Smithsonian Center for Astrophysics, Cambridge, MA, USA
[b]Pennsylvania State University, University Park, PA, USA

ABSTRACT

Arcus is a mission concept for a next generation X-ray grating spectrometer. It will offer spectral resolution ($\lambda/\Delta\lambda$) greater than 2000 combined with over 500 cm^2 of effective area in the 2.1–2.4 nm bandpass. These capabilities will elucidate the cycle of baryonic matter in and out of galaxies, the means by which supermassive black holes influence their surroundings, and the early formation and evolution of solar systems. We present the overall optical design of the mission, which features four arrays of silicon pore optics modules with four matching arrays of off-plane reflection grating modules. These optics disperse the incident X-rays over the 12 m focal length in four separate conical diffraction patterns onto CCD arrays at the focal plane. Each array of optics is an azimuthal sub-aperture of the typical Wolter telescope design, enabling enhanced spectral resolution due to an asymmetric point spread function. The theoretical spectral resolution, effective area, and alignment tolerances have been determined via raytrace modeling.

Keywords: Arcus, X-ray spectroscopy, X-ray optics, silicon pore optics, off plane reflection gratings

1. INTRODUCTION AND TELESCOPE DESIGN

Arcus will be proposed to the NASA Explorer program as a high-resolution soft X-ray spectroscopy mission. The baseline mission requirements are spectral resolution ($\lambda/\Delta\lambda$) $>$ 2000 in the 2.1–2.4 nm bandpass along with $>$ 500 cm^2 of effective area. Such capabilities will allow, among other things, allow the detection and investigation of the hot, low density gas believed to exist in the outskirts of galaxies and clusters. A description of the mission concept can be found in Smith et al. (2016, this volume), and details on the scientific applications in Brenneman et al. (2016, this volume).

The major elements comprising the Arcus X-ray spectrometer are the imaging optics, the diffractive optics, and the focal plane detectors. We use silicon pore optics[1] (SPO), planned for use in the upcoming ATHENA observatory,[2] as the imaging optics. In fact, we will use the exact same 12 m focal length modular design as with ATHENA in order to minimize cost and development time. Off-plane reflection gratings[3] will disperse the converging X-ray beam into a conical diffraction pattern at the focal plane. Arrays of CCDs will cover the 4.2–8.4 nm bandpass in first order, putting the key bandpass toward the long wavelength end of third order.

Off-plane or conical diffraction is less widely understood than the classical in-plane geometry, so we briefly review it before describing the Arcus optical design in detail. Figure 1 shows the geometry of a stacked off-plane grating (OPG) array intended to disperse a converging beam from an imaging telescope. The beam is incident on the array at a shallow graze angle in order to preserve reflectivity as with conventional X-ray optics. The grooves are nearly parallel to the incident beam, which results in diffraction out-of-plane. The telescope focus is specularly reflected to the zero order position, while the diffracted light is spread out in a pattern similar to a cone, hence the conical diffraction nomenclature. The grooves are ideally radial, all directed toward a common point (the hub) at the focal plane.[4,5] This mitigates aberrations due to the incident beam's convergence. The grooves are blazed in order to maximize efficiency to one side of zero order. Finally, the gratings must all have sufficiently flat figure and be aligned such that the diffracted spectra all overlap at the focal plane.

Groupings of SPO modules will be aligned together about a common focus to produce a 'petal.' The petal optical area spans roughly 320–810 mm radially and 360 mm in the azimuthal direction, while the mechanical dimensions are larger as indicated in Fig. 2. A petal of OPG modules of roughly the same size is aligned to the

Space Telescopes and Instrumentation 2016: Ultraviolet to Gamma Ray, edited by
Jan-Willem A. den Herder, Tadayuki Takahashi, Marshall Bautz, Proc. of SPIE Vol. 9905, 99054O
 · doi: 10.1117/12.2233763

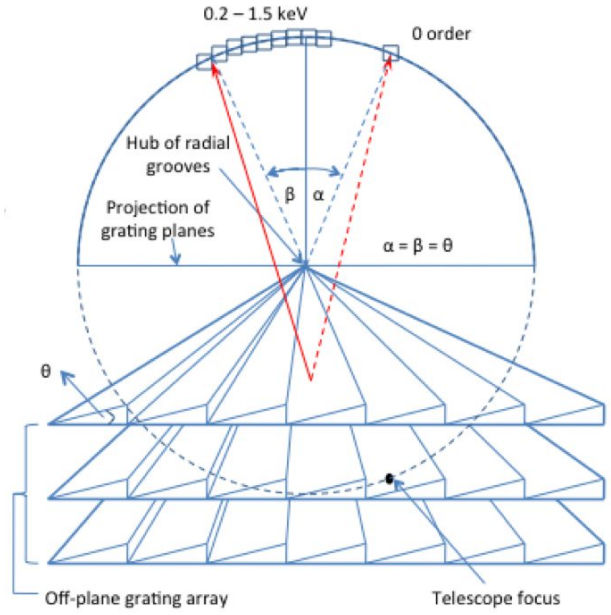

Figure 1. A depiction of stacked off-plane reflection gratings. The grooves are radial and all point towards the common point known as the hub. The grooves are blazed to maximize diffraction efficiency to one side of zero order.

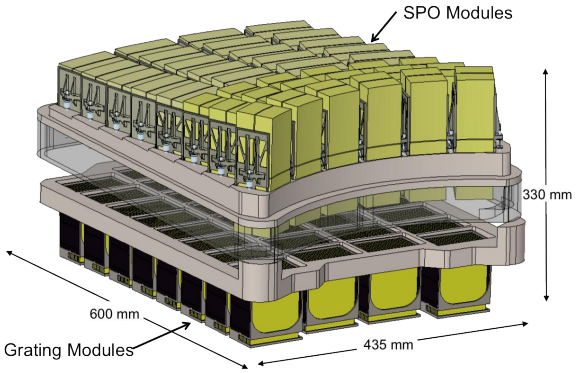

Figure 2. A CAD model of a single Arcus channel. SPO modules are aligned about a common optical axis into a petal. OPG modules are then placed below each SPO module and aligned about the hub. The two petals form the channel.

SPO petal to form a 'channel.' There are four total channels, and the optical layout is shown in Fig. 3. The OPGs reflect the zero order back under the footprint of the channels and then diffract light toward the center of the telescope. Two channels are blazed oppositely so that they diffract onto the same detector array. This minimizes the total number of CCDs required to cover our bandpass. A CAD model of the Arcus mission is depicted in Fig. 4, where only half of the channels are shown, both diffracting to the same focal plane array.

2. OPTICAL PRESCRIPTION

In a nested Wolter telescope, the focal length is defined from the (often imaginary) intersection point between the primary and secondary reflective surfaces.[6] For a given shell, this intersection point can be referred to as a node. The surface on which the nodes lie is called the principle surface. If all nodes in the telescope have the same focal length and are placed on a planar principle surface orthogonal to the optical axis, then the distance from the node to the focus increases with the node radius. This results in a non-uniform plate scale across the telescope, which can dramatically degrade off-axis performance. Therefore, the nodes of the ATHENA (and therefore Arcus) SPO modules will exist on a spherical principle surface centered about the focus.[7]

As mentioned earlier, the grooves of the off-plane gratings must be radially directed toward a point called the hub which is located very near the focal plane (see the Appendix in Ref. 5 for details). For cost reasons, all Arcus gratings in a given channel will be fabricated in an identical fashion, and therefore will have identical groove patterns. Thus, in order to meet the criterion of all grooves pointing to the hub, the OPG modules must also exist on a spherical surface, in this case centered about the hub.

The hub is displaced from the focus by 1.5 degrees in the cross-dispersion plane in order to establish the 1.5 degree incidence angle of the converging beam with the grating surfaces. The SPO and OPG principle surfaces are shown in Fig. 5 in the cross-dispersion plane. The SPO focus, grating hub, and location of the diffraction arc

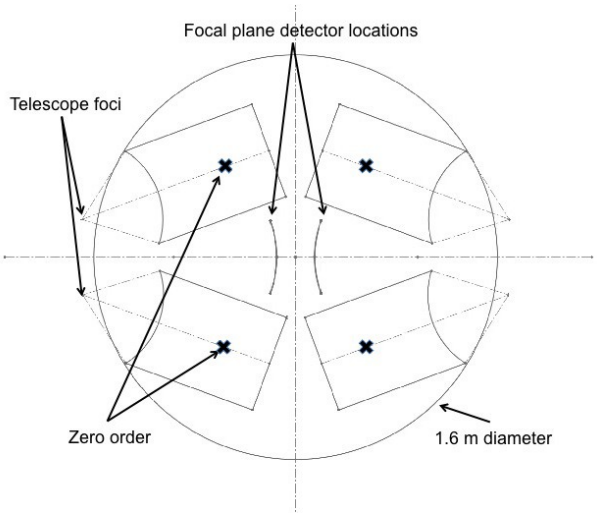

Figure 3. A top-down view of the Arcus layout. The two channels on the left diffract to the same focal plane detector array. The locations of the SPO foci are indicated for these same channels, though the presence of the OPG modules results in a zero order reflection existing underneath the optical aperture.

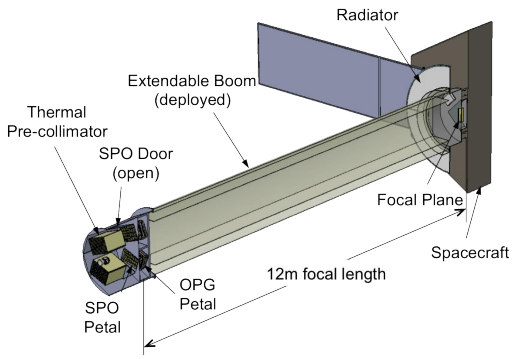

Figure 4. A cross-section of the Arcus mission CAD model. Two channels are shown which diffract to a single focal plane array.

also shown, along with dashed lines indicating the physical extent of the optics. Note that the principle surfaces are shown with far greater lateral extents in order to illustrate their curvatures.

The key Arcus bandpass is near the highly ionized oxygen line at 2.4 nm. In order to maximize the mission effective area in this wavelength region, we have chosen to use the Littrow configuration for 2.4 nm in the third diffraction order. In the notation of Fig. 1, Littrow configuration is when $\alpha = \beta = \theta$, or when the angles of the reflected beam, diffracted beam, and groove facet with respect to the grating normal are all equal when projected in a plane orthogonal to the groove direction. This shifts the blaze function to peak about the desired bandpass, and theoretically maximizes the achievable diffraction efficiency.[8] For our groove period (160 nm), incidence angle (1.5 degrees), and 2.4 nm, third order bandpass, this requires the OPG principle surface be rotated in the dispersion direction by 1.29 degrees as shown in Fig. 6. This angle can be calculated by methods reported in Ref. 9. Figure 7 shows the location of the SPO focus, the zero order reflection, the diffraction arc covered by CCDs, and the location of the 2.4 nm, third order diffraction spot, and one can see the similarities to the Littrow configuration shown in Fig. 1.

The ideal diffraction geometry can only be achieved for a single point on the OPG principle surface. This point is the origin of the 1.5 and 1.29 degree rotations described in the previous two paragraphs, and is defined at the center of the outermost grating surface with respect to the SPO optical axis. As the lateral extent (orthogonal to the SPO optical axis) of the surface increases from this point, the ideal locations of the hubs from the various gratings begin to diverge. For our relatively slow optical system, however, this is a minor effect and the origin of the rotations can practically be chosen at any grating surface. It is possible that a slight perturbation of the OPG principle surface from a sphere may reduce aberrations along the diffraction arc, but the gains are likely to not warrant the addition of mission complexity. This is a subject for future study, though the current prescription meets mission requirements as shown in Sec. 4.1.

3. SUBAPERTURING

As shown in Fig. 3, the SPO modules are not placed symmetrically about the optical axis. Instead, they only span a small ($\lesssim$ 70 degrees) azimuthal portion of a full shell telescope. The inner SPO modules fill a larger angular aperture than the outer modules, while the spatial extent in the direction orthogonal to the central radius is roughly constant. This is motivated by a well-known asymmetry in the point spread function of

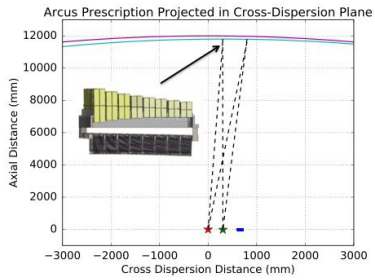

Figure 5. The Arcus optical prescription projected in a plane parallel to the cross-dispersion axis. The location of the SPO focus is shown as a red star, the hub is shown as a green star, and the diffraction arc is plotted in blue. The dashed lines are drawn from the Arcus optical aperture to the focus and the hub. The SPO and OPG principle surfaces are shown across a 6 m distance so that their relative tilt is obvious.

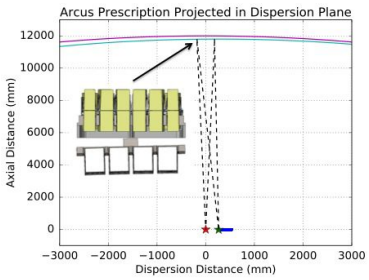

Figure 6. The Arcus optical prescription projected in a plane parallel to the dispersion axis. The symbols are the same as in Fig. 5. The tilt between the SPO focus and the hub is due to the yaw of the grating petal required to achieve Littrow configuration.

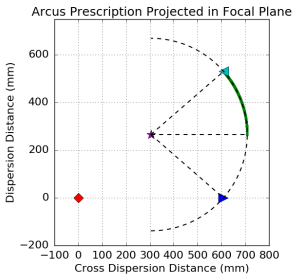

Figure 7. The Arcus optical prescription projected in the focal plane. The red diamond is the SPO telescope focus, the blue triangle is the zero order reflection, and the cyan triangle is the 2.4 nm, third order diffraction spot. The hub is shown as the purple star. The 4.2–8.4 nm first order bandpass is plotted in green. This diagram should be compared to Fig. 1, as both depict the Littrow configuration.

grazing incidence optics. Both geometric aberrations due to low frequency figure error and scattering due to high frequency microroughness occur predominantly in the in-plane direction with a theoretical in-plane to out-of-plane ratio of $1/\sin\theta$. Thus, as the azimuthal extent of a grazing incidence telescope is reduced, the PSF becomes narrower in the out-of-plane direction. The PSF collapsed in this direction is frequently referred to as a line spread function (LSF). While the theoretical improvement in LSF for a subaperture of θ is $1/\theta$,[10] the practical improvement is typically less. This is believed to be due to anisotropy in the surface statistics of low frequency figure error; more effort is made to reduce axial figure error than azimuthal figure error because most Wolter optics are designed to be incorporated into full telescope shells.

By design, the dispersion axis of the OPG modules is orthogonal to the mean radial direction of the SPO modules. This means that the X-rays are dispersed in the narrow direction of the telescope PSF as indicated in Fig. 8. The fact that the LSF is much narrower than the in-plane PSF increases the resulting spectral resolution. It should be noted that the azimuthal extent of the Arcus optics modules also results in focus error at high dispersions. X-rays from one side of the channel travel a different distance to the focal plane than X-rays from the other side. This results in aberrations due to the finite telescope depth-of-focus. Thus, at large SPO radii the spatial extent of the subaperture dominates the resulting LSF aberrations, whereas at small SPO radii the angular extent of the subaperture dominates. Figure 9 demonstrates this concept, and likely represents the ideal subaperture shape for a mission like Arcus. To make packing the channels into the layout shown in Fig. 3 easier, however, we have chosen a roughly rectangular subaperture.

4. RAYTRACE RESULTS

The Arcus optical design was raytraced using custom software written in Python and Fortran. Rays are generated at the SPO primary surfaces and assigned a wavelength and a weight based on the geometric collecting area of the SPO modules. At each surface, the weight is multiplied by reflectivity or diffraction efficiency where appropriate. The SPO surfaces are assumed to be coated with 15 nm of Ir followed by 8 nm of B_4C with 0.5 nm RMS microroughness, with reflectivities computed using the IMD software package.[11] The carbon based overcoat was studied for use in ATHENA to boost low energy reflectivities.[12] The PCGrate software package was used to compute diffraction efficiencies, and a 15 nm Au coating with 3 nm RMS microroughness is assumed. This microroughness value was found to fit empirical efficiency measurements for prototype OPGs.[13] After the rays are traced to the focal plane, the weights are multiplied by factors to account for SPO module to OPG

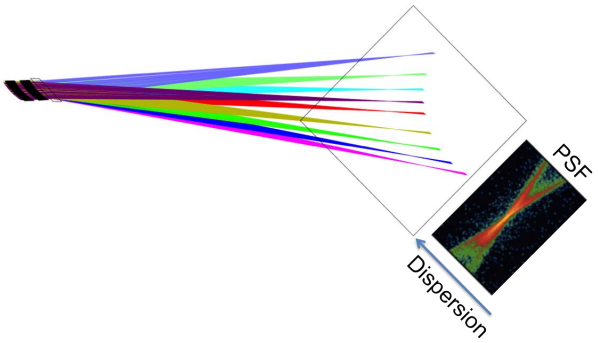

Figure 8. A depiction of the off-plane reflection grating spectrometer concept. The black surfaces represent a Wolter mirror pair, followed by a rectangle representing an off-plane grating. The large square indicates the focal plane, onto which the gratign produces a conical diffraction pattern. The PSF in this geometry is narrow in the dispersion direction, permitting higher spectral resolving powers.

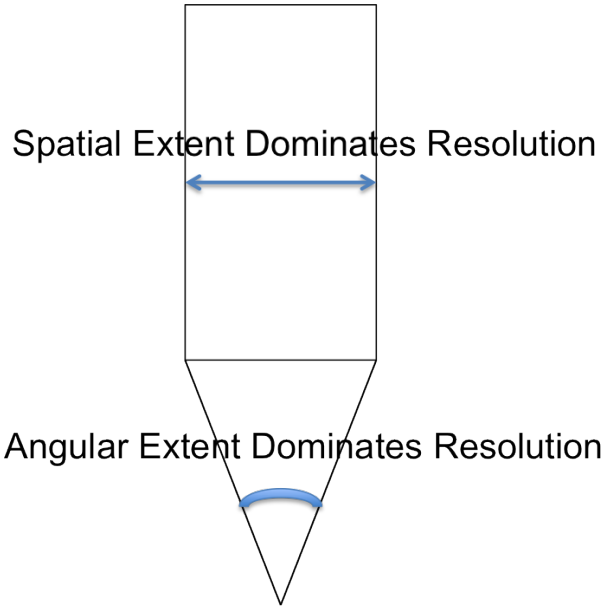

Figure 9. The aperture chosen for a mission like Arcus depends on both focus errors and the angular extent of the telescope PSF. The vertical and horizontal directions correspond to the telescope radial and azimuthal directions, respectively. At inner radii, the angular broadening of the telescope PSF dominates the resolving power. At outer radii, the path length differences from one azimuthal side to the other as light is diffracted away from zero order dominates the resolving power.

module mechanical layout mismatch, the thickness of the SPO ribs and OPG substrates, the transmission of CCD filters, and CCD quantum efficiency.

4.1 Resolution and Throughput

The Arcus raytrace only includes the aberrations inherent to the optical design. In other words, the optical surfaces are modeled as being perfectly figured. To estimate LSFs (and therefore resolution) over the diffraction arc, the weighted ray positions were binned in the dispersion direction and convolved with a Gaussian representing scatter, misalignment terms, fabrication errors, etc. The contribution from the SPO optics was assumed to be a 1.5 arcsecond FWHM Gaussian, and the contribution from all other sources was taken to be a 2 arcsecond FWHM Gaussian. Reported resolutions in Fig. 10 are $\lambda/\Delta\lambda$, where $\Delta\lambda$ is the FWHM. Effective area is shown in 11, and is the summation of all weights as described above for a given wavelength and order.

4.2 Focal Plane Curvature

In a fashion similar to conventional Wolter telescopes, the ideal focal plane for an Arcus channel curves up toward the optics as light is diffracted farther away from zero order. To maximize spectral resolution, the CCDs should be positioned to match this curvature as closely as possible. This is not strictly possible for Arcus, however, because two channels diffract onto a single CCD array. The spectra from these two channels are reversed so that the short wavelength region of one channel is the long wavelength region of the other channel. Thus, the two channels have opposing ideal focal plane curvatures. We have chosen to place the nominal Arcus focal plane to maximize spectral resolution at 2.4 nm in the third order for both channels. This situation is illustrated in Fig. 12, though in a simplified geometry.

The depth of focus is plotted as spectral resolution vs. axial focal plane offset in Fig. 13 for the short (2.1 nm), middle (3.15 nm), and long wavelength (4.2 nm) regions of the arc in second order. Also plotted is the

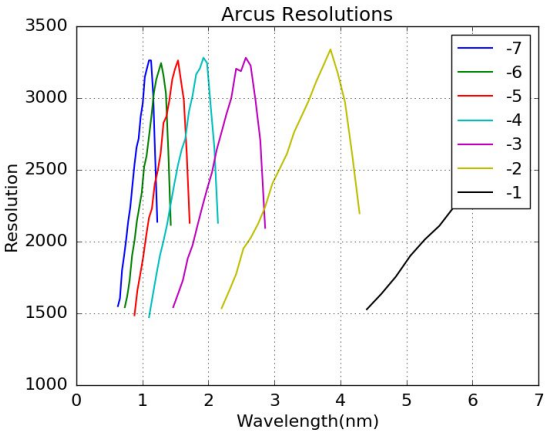

Figure 10. The spectral resolving power ($\lambda/\Delta\lambda$) of the Arcus optical design. $\Delta\lambda$ is the LSF FWHM, and includes an assumed 1.5 arcsecond SPO contribution and a 2 arcsecond static and dynamic misalignment contribution.

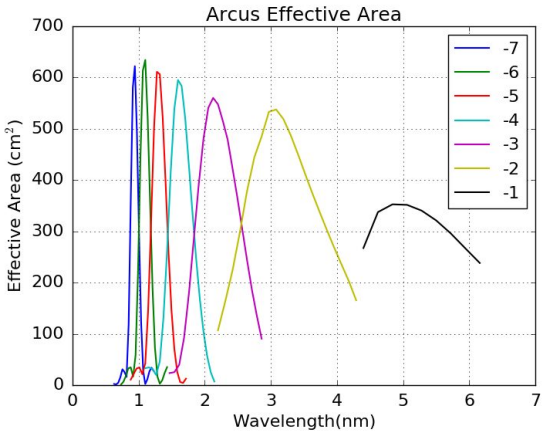

Figure 11. The effective areas for the four channel Arcus optical design.

depth of focus for the 2.4 nm, third order optimization wavelength. These results show that the Arcus depth of focus is on the order of 10 mm for the optimization wavelength, and that there would not be a significant boost in resolutions at lower wavelengths if focal plane curvature was introduced. It could be possible to shift the focal plane closer to the optics in order to take advantage of high resolving powers at longer wavelengths, and with some curvature toward the middle of the focal plane retain resolution across the rest of the Arcus bandpass. This concept is indicated by the "Optimized Focal Plane" in Fig. 12.

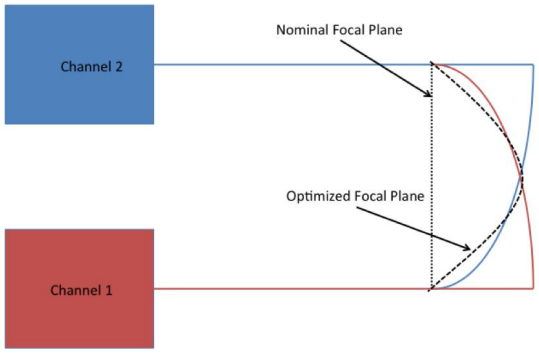

Figure 12. A conceptual diagram of the depth of focus for a single focal plane detector array. The diffraction arcs from the two contributing channels have opposite curvatures. The nominal focal plane is a plane orthogonal to the optical axis, optimized for 2.4 nm, third order diffraction. A slight bow could be introduced to potentially increase resolution at long wavelengths while retaining resolving power toward the middle of the arcs.

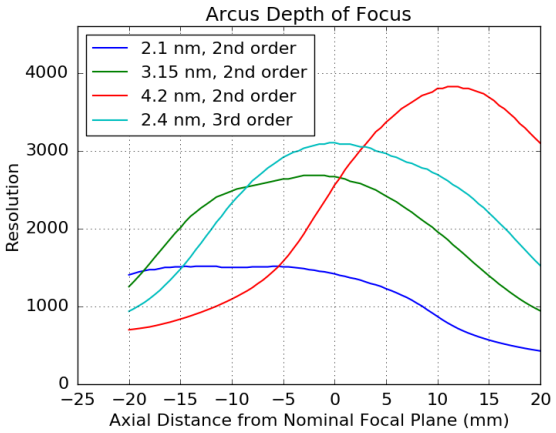

Figure 13. A plot of the resolution as a function of focal plane axial offset for various wavelengths. The second order plots are at the short, medium, and long wavelength regions of the arc. The 2.4 nm, third order diffraction for which the focal plane is optimized is also plotted for convenience.

4.3 Off-Axis Behavior

In a conventional Wolter telescope, an off-axis pointing shifts the image point by $F\theta$, where F is the focal length and θ is the off-axis angle. In this respect, the Wolter mirror pairs essentially act as a thin lens. For Arcus, the addition of the third optical surface (the gratings) modifies this behavior due to the grazing incidence off-plane diffraction geometry. This can be qualitatively understood by considering the focal plane diagram in Fig. 7. The SPO focus is shifted due to an off-axis pointing in the conventional manner, while the location of the hub is constant. The location of zero order shifts by the same amount in the dispersion direction and the opposite amount in the cross-dispersion direction. The radius of the diffraction arc is equal to the distance from the hub to zero order or, equivalently, the SPO focus. Thus, a spacecraft pointing offset in either the dispersion or cross-dispersion axes changes the radius of the arc. Finally, for small rotations the amount of dispersion per unit wavelength in the dispersion axis is constant. In other words, the distance between zero order and a diffraction spot of a given order and wavelength, both projected on the dispersion axis, does not change for small ($\lesssim 1$ degree) pointing offsets. Also note that there are two channels diffracting to a single detector array, and that the dispersion axes are at an oblique angle to one another. This means that the two arcs will not move in the same manner under changes in spacecraft pointing.

Figure 14 shows the motion of the arc for the two rotations as computed using the raytrace model. The location of the diffraction arc from 4.2–8.4 nm in first order is shown for an on-axis pointing for reference. The effect of a 10 arcminute off-axis angle is shown for pointing offsets in the dispersion (yaw) and cross-dispersion (pitch) directions with arbitrary sign conventions. The negative pitch offset shifts the SPO focus in the positive cross-dispersion direction. This shifts zero order in the negative cross-dispersion direction and reduces the radius of the arc (refer to Fig. 7). The positive pitch offset has the opposite effect. The negative yaw offset results in a shift of both the SPO focus and zero order in the negative dispersion direction. This increases the arc radius and also shifts the 4.2–8.4 nm bandpass by the same amount in the negative dispersion direction. Note that this shift of the bandpass must still occur along the diffraction circle, and that it is the bandpass projected along the dispersion axis that shifts by the same amount as zero order. The increased arc radius is the reason for the positive cross-dispersion shift due to a negative yaw pointing offset. The situation is, of course, reversed for the positive yaw pointing offset.

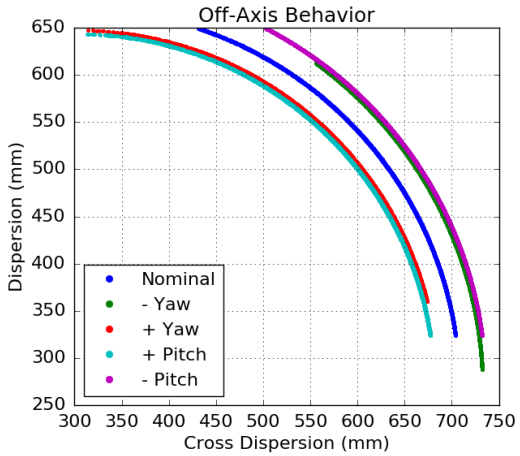

Figure 14. The shift of the diffraction arc under yaw and pitch pointing offsets of the spacecraft. The pointing offsets shown are 10 arcminutes.

4.4 Alignment Tolerances

The Arcus raytrace model has been used to investigate optical alignment tolerances as in Ref. 14. Because we are primarily concerned with preserving spectral resolution, there are only three degrees of freedom that must be constrained with extreme precision. These are the SPO module translation in the dispersion direction, the

SPO module roll about the optical axis, and the OPG module roll about the optical axis (with the origin of rotation being at the module). These three degrees of freedom must be constrained to 5 μm, 5 arcseconds, and 5 arcseconds, respectively. These are approximate tolerances, and may vary somewhat depending on the size of the other terms in the LSF error budget. Optical methods have been developed to achieve these tolerances, and have been reported on in Refs. 15. Alignment tolerances required for all other degrees of freedom associated with placement of the SPO and OPG modules will be achieved with standard machining tolerances and verified at subassembly alignment.

ACKNOWLEDGMENTS

This work has been supported by NASA grants NNX12AI16G, NNX12AF23G, NNX13AD03G, NNX15AC42G, and internal Smithsonian funding.

REFERENCES

[1] Collon, M. J., Vacanti, G., Günther, R., Yanson, A., Barrière, N., Landgraf, B., Vervest, M., Chatbi, A., Beijersbergen, M. W., Bavdaz, M., Wille, E., Haneveld, J., Koelewijn, A., Leenstra, A., Wijnperle, M., van Baren, C., Müller, P., Krumrey, M., Burwitz, V., Pareschi, G., Conconi, P., and Christensen, F. E., "Silicon pore optics development for ATHENA," in [*Society of Photo-Optical Instrumentation Engineers (SPIE) Conference Series*], *Proc. SPIE* **9603**, 96030K (Sept. 2015).

[2] Nandra, K., "Athena: Exploring the Hot and Energetic Universe," in [*AAS/High Energy Astrophysics Division*], *AAS/High Energy Astrophysics Division* **14**, 301.01 (Aug. 2014).

[3] McEntaffer, R., DeRoo, C., Schultz, T., Gantner, B., Tutt, J., Holland, A., O'Dell, S., Gaskin, J., Kolodziejczak, J., Zhang, W. W., Chan, K.-W., Biskach, M., McClelland, R., Iazikov, D., Wang, X., and Koecher, L., "First results from a next-generation off-plane X-ray diffraction grating," *Experimental Astronomy* **36**, 389–405 (Aug. 2013).

[4] Cash, Jr., W. C., "X-ray spectrographs using radial groove gratings," *Applied Optics* **22**, 3971–3976 (Dec. 1983).

[5] Flanagan, K. A., Davis, J. E., Heilmann, R. K., Levine, A. M., McGuirk, M., Ricker, G. R., Schattenburg, M. L., Wise, M., Rasmussen, A., Bookbinder, J. A., Freeman, M. D., Gaetz, T. J., Jerius, D., Nguyen, D., Podgorski, W. A., Reid, P. B., Cash, W. C., Shipley, A. F., Gallagher, D. J., Huang, P., and Jordan, S. P., "The Constellation-X RGS options: raytrace modeling of the off-plane gratings," in [*UV and Gamma-Ray Space Telescope Systems*], Hasinger, G. and Turner, M. J. L., eds., *Proc. SPIE* **5488**, 515–529 (Oct. 2004).

[6] van Speybroeck, L. P. and Chase, R. C., "Design parameters of paraboloid-hyperboloid telescopes for X-ray astronomy.," *Applied Optics* **11**, 440–445 (1972).

[7] Willingale, R., Pareschi, G., Christensen, F., and den Herder, J.-W., "The Hot and Energetic Universe: The Optical Design of the Athena+ Mirror," *ArXiv e-prints* (July 2013).

[8] Neviere, M., Maystre, D., and Hunter, W. R., "On the use of classical and conical diffraction mountings for XUV gratings," *Journal of the Optical Society of America (1917-1983)* **68**, 1106–1113 (Aug. 1978).

[9] DeRoo, C. T., McEntaffer, R. L., Miles, D. M., Peterson, T. J., Marlowe, H., Tutt, J. H., Donovan, B. D., Menz, B., Burwitz, V., Hartner, G., Allured, R., Smith, R. K., Gunther, R., Yanson, A., Vacanti, G., and Ackermann, M., "Line Spread Functions of Blazed Off-Plane Gratings Operated in the Littrow Mounting," *ArXiv e-prints* (Mar. 2016).

[10] Cash, W., "X-ray optics - A technique for high resolution imaging," *Applied Optics* **26**, 2915–2920 (July 1987).

[11] Windt, D. L., "IMD–Software for modeling the optical properties of multilayer films," *Computers in Physics* **12**, 360–370 (July 1998).

[12] Ferreira, D. D. M., Christensen, F. E., Jakobsen, A. C., Westergaard, N. J., and Shortt, B., "ATHENA optimized coating design," in [*Space Telescopes and Instrumentation 2012: Ultraviolet to Gamma Ray*], *Proc. SPIE* **8443**, 84435L (Sept. 2012).

[13] Marlowe, H., McEntaffer, R. L., Tutt, J. H., DeRoo, C. T., Miles, D. M., Goray, L. I., Soltwisch, V., Scholze, F., Herrero, A. F., and Laubis, C., "Modeling and empirical characterization of the polarization response of off-plane reflection gratings," *Appl. Opt.* **55**, 5548–5553 (Jul 2016).

[14] Allured, R. and McEntaffer, R. T., "Analytical alignment tolerances for off-plane reflection grating spectroscopy," *Experimental Astronomy* **36**, 661–677 (Dec. 2013).

[15] Allured, R., Donovan, B. D., DeRoo, C. T., Marlowe, H. R., McEntaffer, R. L., Tutt, J. H., Cheimets, P. N., Hertz, E., Smith, R. K., Burwitz, V., Hartner, G., and Menz, B., "Optical and x-ray alignment approaches for off-plane reflection gratings," in [*Society of Photo-Optical Instrumentation Engineers (SPIE) Conference Series*], *Proc. SPIE* **9603**, 960315 (Sept. 2015).